PERFORMANCE ANALYSIS OF A SCRAMJET INLET-ISOLATOR USING EXPERIMENTAL & NUMERICAL METHODS

A. Che Idris, M. R. Saad, H. Zare-Behtash, E. Erdem & K. Kontis
University of Manchester
Azam.cheidris@postgrad.manchester.ac.uk

Abstract

Experimental and numerical investigations were conducted to understand the complex flow features inside a generic two dimensional planar scramjet inlet-isolator. The inlet-isolator was designed to satisfy the ideal condition of Shock-on-Lip (SOL) in Mach 5 inviscid flow. Angle of attack was varied to simulate off-design flight conditions for the inlet-isolator. Numerical methods were used to estimate various performance indicators at different test conditions. The changes in inlet efficiencies were shown to be heavily influenced on the flow quality inside the isolator.

1 Introduction

For practical reason, a scramjet inlet-isolator is optimised for operation at one specific flight condition which is usually the cruise condition where the aircraft will spend most of its flying time. However at off-design conditions, many adverse flow conditions could occur whereby reducing its performance or even inducing inlet un-start.

Bachchan and Hillier [1] tries to classify different inlet off-design conditions into five main types depending on the combinations of shocks from forebody and cowl segment. Many studies has been conducted to investigate the relationship between inlet flowfield and different off-design variables such as flight Mach number [1], angle of attack (AoA) [2], yaw angle [3], and freestream air temperature [4][5][6][7][8].

However, there is a serious lack of references discussing the effect of angle of attack on scramjet inlet performance even though a scramjet aircraft would certainly change its angle of attack sometimes during its overall flight trajectory. Thus this paper seeks to contribute to the overall body of knowledge by conducting experimental and numerical investigations relating to the subject matter.

Three most common scramjet inlet performance indicators are Total Pressure Ratio, Kinetic Energy Efficiency and Dimensionless Entropy Increase [9]. Total Pressure Ratio shows the fraction of total pressure still available in the flow after the compression process. Typically a hypersonic inlet will exhibit lower value of Total Pressure Ratio if compared to a supersonic inlet [9].

Kinetic Energy Efficiency on the other hand demonstrates the potential flow velocity obtainable if the compressed flow in throat section were to be isentropically expanded without combustion. It is referenced to freestream flow velocity and usually has a very close value to unity [9].

Since severe interactions of shocks and boundary layer are expected in a hypersonic inlet, a good measure of irreversibility is done by calculating the Dimensionless Entropy Increase. A high quality flow would have a low value of entropy increase [9].

Using a validated numerical simulation to calculate the inlet performance simplifies inlet parametric studies without the need to perform many invasive measurement techniques and experiments.

2 Experimental Setup

2.1 High Supersonic Tunnel

The experiments were carried out in High Supersonic Tunnel (HSST) producing Mach 5 flow with Reynolds number of 13.2×10^6 m^{-1}. The blow down tunnel has stagnation pressure of 6.50 bar (±0.05 bar) and stagnation temperature of 375 K (±5 K). The setup is similar to the one used in reference [10] (see Fig. 1).

2.2 Scramjet Inlet-isolator Model

The intake model consisted of a double ramp with see through cowl segment. It was designed to satisfy Shock-on-Lip condition in inviscid Mach 5 flow. The overall length, height and width of the inlet-isolator model is 155 mm × 33.6 mm × 36 mm.

In this investigation, inlet-isolator model was subjected to three different angle of attacks of 0 (baseline), 2 and 4 degree respectively.

10 pressure tappings are installed alongside the middle line of the model connected to Kulite Static Pressure Transducer.

The material used for double ramp and cowl frame is aluminium alloy while the cowl window segments are made from Perspex. The digram is shown in Fig. 2.

2.3 Colour Schlieren Setup

The schlieren system used is a Toepler's z-type such as the one used in [11]. The system is consisted of a 300 W continuous Xenon Arc Lamp with focusing lens and a 2mm wide slit, two parabolic mirrors, tri-coloured knife edge and a set of Hoya 49mm lenses for image focusing. The camera used is Canon EOS-450D 12 MP set at continuous shot of 3.5 frames per second.

2.4 Numerical Methods

Favre Averaged Navier-Stokes (FANS) equations are solved by using density based commercial solver Fluent. Second order spatially accurate scheme are utilized together with Roe's Flux-Difference Splitting.

Menter's Shear-Stress Transport κ-ω are selected as the main turbulence model as it has been repeatedly validated by previous experiments performed using the HSST [12]. For the range of Reynolds number obtainable from the HSST, laminar flow is expected unless tripped thus transitional flow option is selected in the solver [12].

Air is specified as ideal gas and Sutherland Law is used to calculate the viscosity. The boundary condition at Freestream and Inflow are specified using HSST test section's condition whilst the Outflow properties are extrapolated from the interior. Constant temperature is used at the solid walls.

Inviscid solution was used as the initialization value for the turbulence simulation. Grid density sensitivity was investigated by using coarse (34,485), medium (52,250) and fine (73,840) grid.

3 Results and Discussions

3.1 Sensitivity Analysis

From Fig. 3 we can conclude that numerical results from Medium and Fine mesh are very similar. Coarse mesh also produces almost similar pattern of pressure peaks in the isolator section (downstream of x = 0.08 m) but the mesh is not fine enough to resolve flow separation around compression corner between first and second ramp. The solution demonstrates grid independent thus allowing the use of Medium grid for all case studies reported herein.

3.2 Numerical Accuracy

Normalized static pressure readings along centerline of the scramjet inlet are plotted in Fig. 7. For all AoA, excellent agreements are present between numerical and experimental data. Qualitatively, density gradient contours plot from numerical simulation are observed to match very closely the flow topology captured by colour schlieren (see Fig. 4, Fig. 5 and Fig.6).

3.3 Baseline Case

Fig. 4 shows complex and comprehensive view of flow topology for a Mach 5 scramjet inlet-isolator with zero degree angle of attack. There are four separation bubbles identified by presence of separation and reattachment shocks.

Separation at compression corner produced Goetler vortices that assist in transition to turbulence [13]. Separation and reattachment shocks from the separation bubble intersect each other to form Edney's Type VI shock interaction. Since both of Separation Shock and Reattachment Shock are from the same family (i.e. have the same shock direction), a stronger shock and expansion wave is produced from the point of interaction with the flow divided by a slip line. Thus flow downstream of separation is non uniform.

Separation Bubble 1 originating from cowl lip is thought as a product of lip bluntness effect [14]. As lip cannot be made perfectly sharp due to manufacturing constraint, bow shock emerged and gave rise to entropy layer with strong vorticity [15]. Shock from Separation Bubble 2 interacted with this layer resulting in a bubble of recirculated flow [14]. It is an inviscid phenomenon but could appear as boundary layer separation in real life viscous fluid. Lip bluntness effect is not present in the numerical colour schlieren in Fig 4(a). This explains the slight discrepancy in pressure reading between experiments and simulation in Fig. 7.

Interaction between Separation Shock 1 and 2 is identified as Edney's Type 1. Since both of the shock is from different family, it can cross each other. Thus two transmitted shock emerged from the intersection point. Flow downstream of a transmitted shock has different properties except pressure and velocity from the flow downstream of another. This will add to flow non-uniformity and could also cause the flow to become unsteady due to presence of Kelvin-Helmholtz instability at the slip line. [16].

The inlet-isolator is prone to unstart due to presence of Separation Bubble 1 and 2 which increased the contraction ratio. Unstart will occur if contraction ratio goes beyond Kantrowitz limit [17].

3.4 Effects of AoA on Inlet-isolator Flowfield

With increase in AoA, the separation at compression corner decrease in size (see Fig. 4, Fig. 5 and Fig.6). The compression corner's separation shock appeared 'smeared' as the separation become more subtle. Reference [18] has observed that separation at compression ramp became large with unit Reynold's number. In our case, lower flow Mach number experienced by both ramps at higher AoA, reduce the unit Reynolds number. Cowl tip separation also becomes smaller with increasing AoA.

As the inlet increase it AoA the total turning of the flow before it enters the throat also increase thus lowering the entrance Mach number. Low Mach number combined with 'tall' shoulder separation bubble in 4 deg AoA case enabled the formation of Edney's Type II shock-shock interaction (see Fig. 6). It is similar to Edney's Type I interaction where two shock of different family intersect each other but of such strength that a Mach stem must exist between the two shock to enable the required flow turning. Downstream of the Mach stem is a subsonic pocket bounded by two slip lines emanating from the intersections of the Mach stem with the two oblique shocks. Thus the flow is highly non-uniform around the throat area with some part has subsonic speed while the other stays supersonic. However as we can still observe fully established oblique shock train downstream of throat the subsonic flow eventually became supersonic again after it pass the expansion fans around the two separation bubbles.

The shock train inside the isolator section becomes more 'compact' as the shocks reflect in shorter distance with increase in AoA.

3.5 Effects of AoA on Inlet-isolator Performance

Flow properties from the simulation were mass-averaged to calculate Total Pressure Ratio, Kinetic Energy Efficiency and Dimensionless Entropy Increase using equations from [9].

From Fig. 8, Fig. 9 and Fig. 10, it is apparent that scramjet inlet-isolator performance improves slightly with increase in AoA. However, if the AoA is such that a Mach stem is introduced into the flow, the overall performance then dropped quite dramatically.

The improvements in performance by the inlet-isolator at AoA = 2 compared to at AoA = 0 are due to smaller flow separation at compression corner and at cowl tip region. Flow separation introduces unnecessary separation and reattachment shocks which increase the total pressure loss and promotes flow non-uniformity. Smaller separation with weaker separation and reattachment shocks will improve the performance.

On the other hand, appearance of Mach stem (normal shock) in the case of AoA = 4 lower the performance of the inlet significantly. A normal shock is exactly the shock phenomena most unwanted inside a scramjet inlet. It produces unbearable temperature increase and is highly inefficient in compressing air at hypersonic speed. The presence of a subsonic pocket downstream of the normal shock increases flow non-uniformity which will adversely affect combustion performance.

4 Conclusions

The study demonstrates the ability of Fluent to closely predict the flow features of a scramjet inlet-isolator at Mach 5; closely matching the experimental observation. This has enabled a rapid performance comparison of the inlet at various off-design conditions showing the general relations between flow topology and the calculated performance indicators.

The study also shows how significant is the effect of flow separations to the inlet performance. Highly detailed colour schlieren images accompanied by matching numerical simulations are invaluable to an inlet designer in determining how and where to implement flow control for the inlet.

References

[1] Bachchan N and Hillier R. Hypersonic Inlet Flow Analysis at Off-design Condition. *AIAA Paper 2004-5380,* 2004

[2] Boon S and Hillier R. Mach 6 Hypersonic Inlet Flow Analysis at Incidence. *AIAA Paper 2006-3036,* 2006

[3] Hohn O and Gulhan A. Experimental Investigation of the Influence of Yaw Angle on the Inlet Performance at Mach 7. *AIAA Paper 2010-938,* 2010

[4] MacRae DS and Neaves M. Time Accurate Computations of Unsteady Hypersonic Inlet Flows with a Dynamic Flow Adaptive Mesh. *Airforce Office of Scientific Research Final Technical Report,* 1998

[5] Mayer DW and Paynter GC. Prediction of Supersonic Inlet Unstart Caused by Freestream Disturbances. *AIAA Journal,* Vol. 33, No. 2, pp 266-275, 1995

[6] Chang J, Bao W, Yu D, Fan Y, and Shen Y. Effects of Wall Cooling on Performance Parameters of Hypersonic Inlets. *Acta Astronautica,* Vol. 65, pp 467-476, 2008

[7] Lin KC, Tam CJ, Eklund DR, Jackson KR, Jackson and TA. Effects of Temperature and Heat Transfer on Shock Train Structures Inside Constant Area Isolators. *AIAA Paper 2006-817,* 2006

[8] Krause M, Reinartz B and Ballmann J. Numerical Investigation and Simulation of Transition Effects in Hypersonic Intake Flows. *In High Performance Computing in Science and Engineering,* pp 391-406, 2007

[9] Heiser WH and Pratt DT. *Hypersonic Airbreathing Propulsion.* 1st edition, American Institute of Aeronautics and Astronautics, 1994

[10] Erdem E, Yang L and Kontis K. Drag Reduction Studies by Steady Energy Deposition at Mach 5. *AIAA Paper 2011-1027.* 2011

[11] Yang L, Zare-Behtash H, Erdem E, and Kontis K. Application of AA-PSP to Hypersonic Flows: The Double Ramp Model. *Sensor and Actuators B:Chem.* 2011

[12] Erdem E. *Active Flow Control Studies at Mach 5: Measurement and Computation.* PhD Thesis. University of Manchester, 2011

[13] Saric WS. Goetler Vortices. *Ann. Rev. Fluid Mech.* 26, 1994

[14] Boon S and Hillier R. Hypersonic Inlet Flow Analysis at Mach 5, 6 and 7. *AIAA Paper 2006-12,* 2006

[15] Anderson JD. *Hypersonic and High Temperature Gas Dynamics.* American Institute of Aeronautics and Astronautics, 2006

[16] Bertin JJ. *Hypersonic Aerothermodynamics.* American Institute of Aeronautics and Astronautics, 1994

[17] Das S and Prasad JK. Starting Characteristics of a Rectangular Hypersonic Air Intake with Cowl Deflection. *The Aeronautical Journal,* 114, pp 177-189, 2010

[18] Matsumura S, Schneider SP and Berry SA. Streamwise Vortex Instability and Transition on the

Hyper-2000 Scramjet Forebody. *Journal of Spacecraft and Rockets,* 42, 2005

Copyright Statement

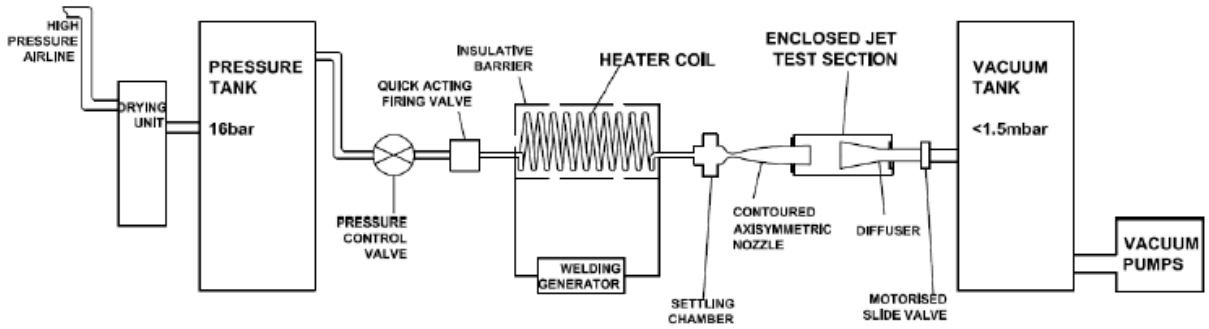

Fig. 1. High Supersonic Wind Tunnel (HSST) setup [10]

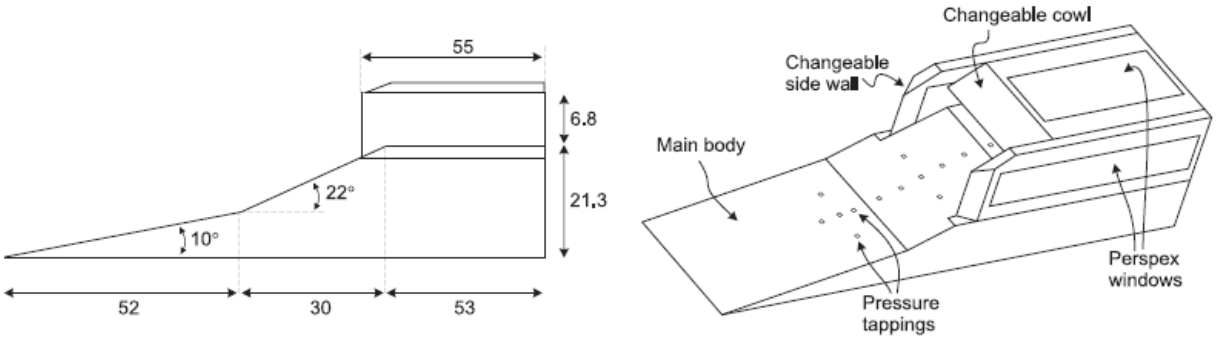

Fig. 2. Schematic diagram of scramjet inlet-isolator model

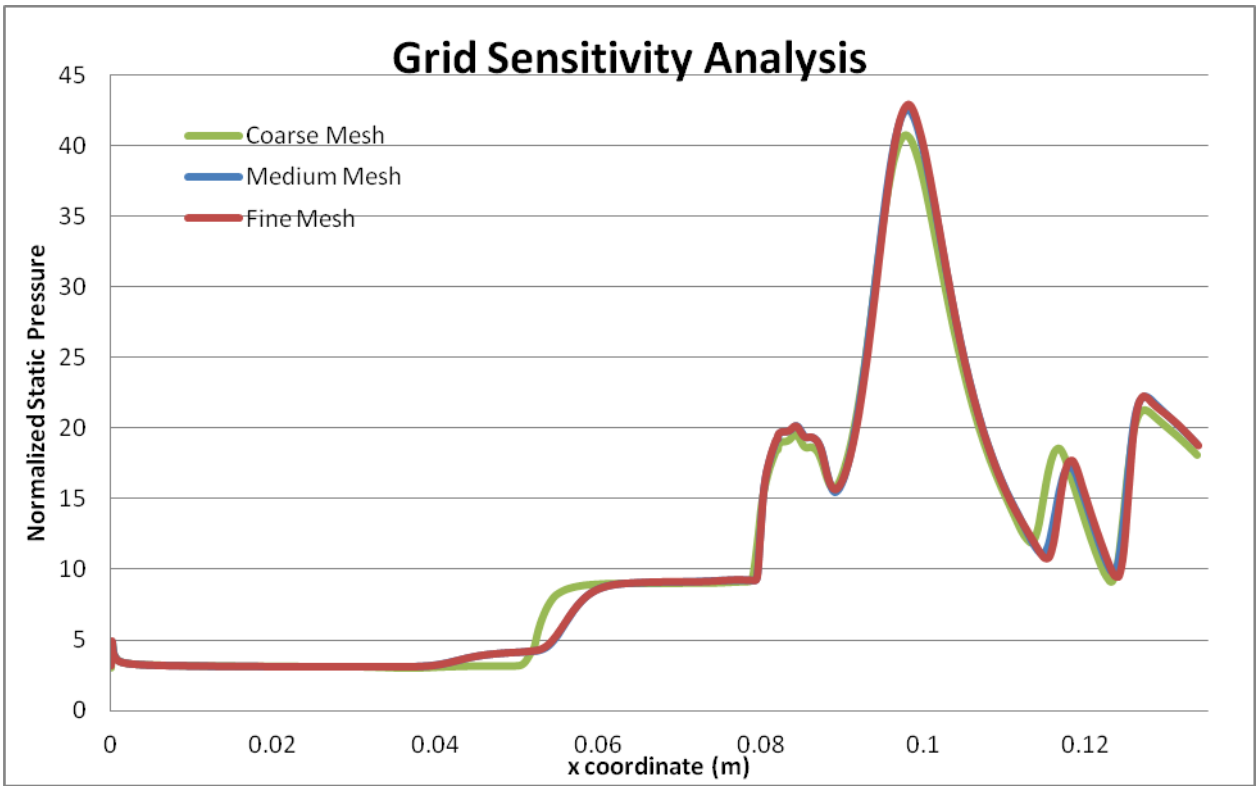

Fig. 3. Plot of normalized pressure of scramjet inlet-isolator model using coarse, medium and fine mesh

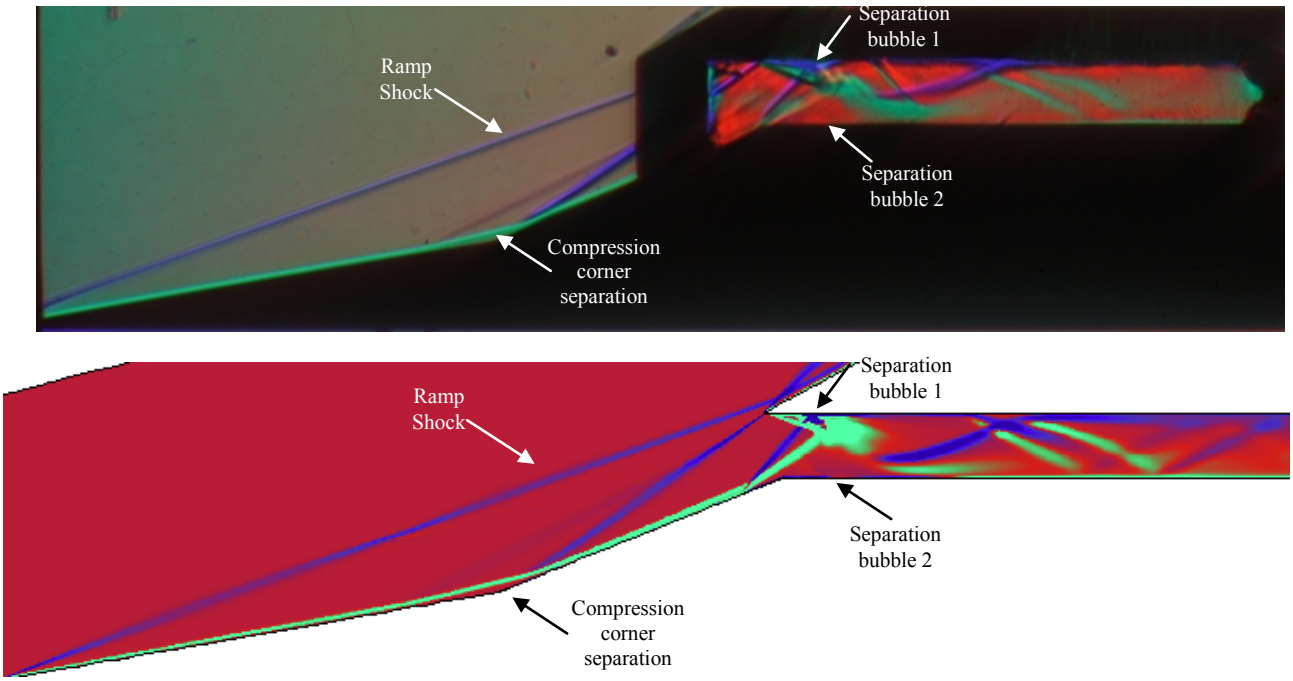

Fig. 4. [Top] Colour schlieren image of baseline case. [Bottom] Numerical colour schlieren of baseline case

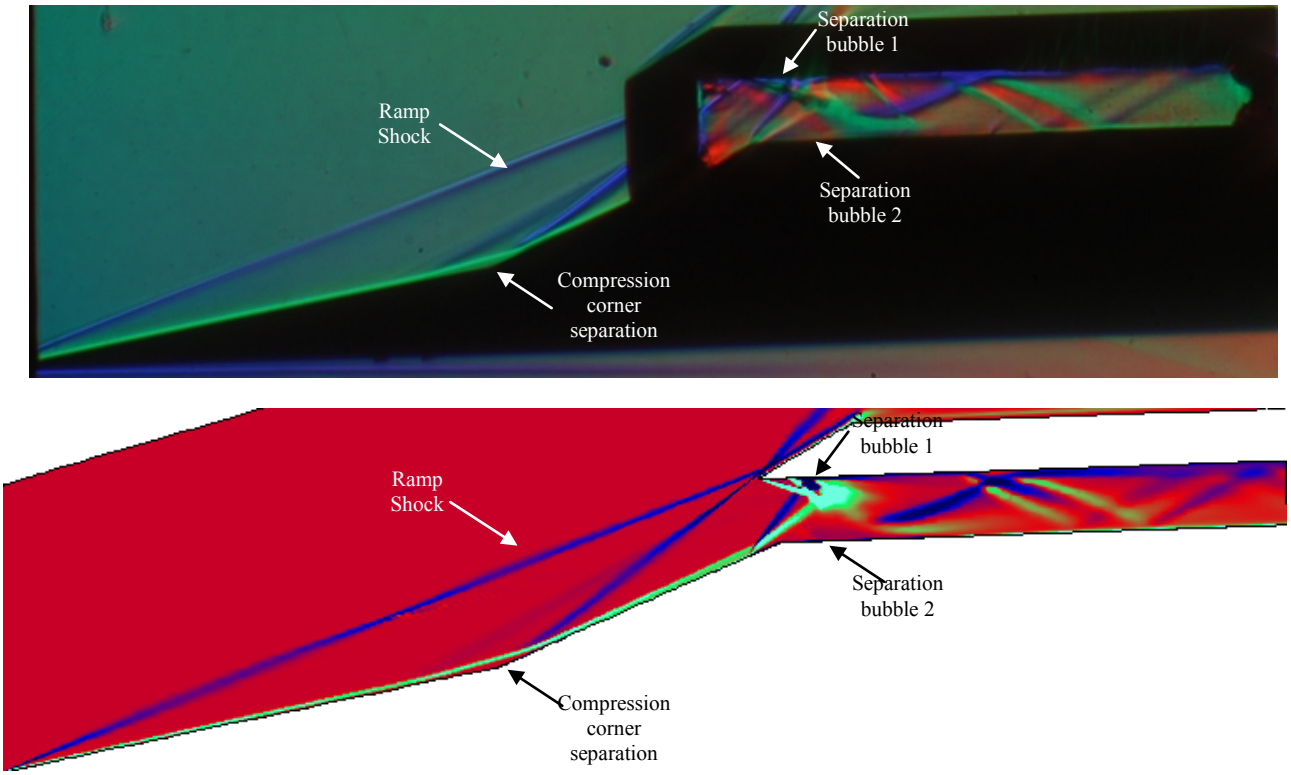

Fig. 5. [Top] Colour schlieren image of AoA = 2deg case. [Bottom] Numerical colour schlieren of AoA = 2deg case

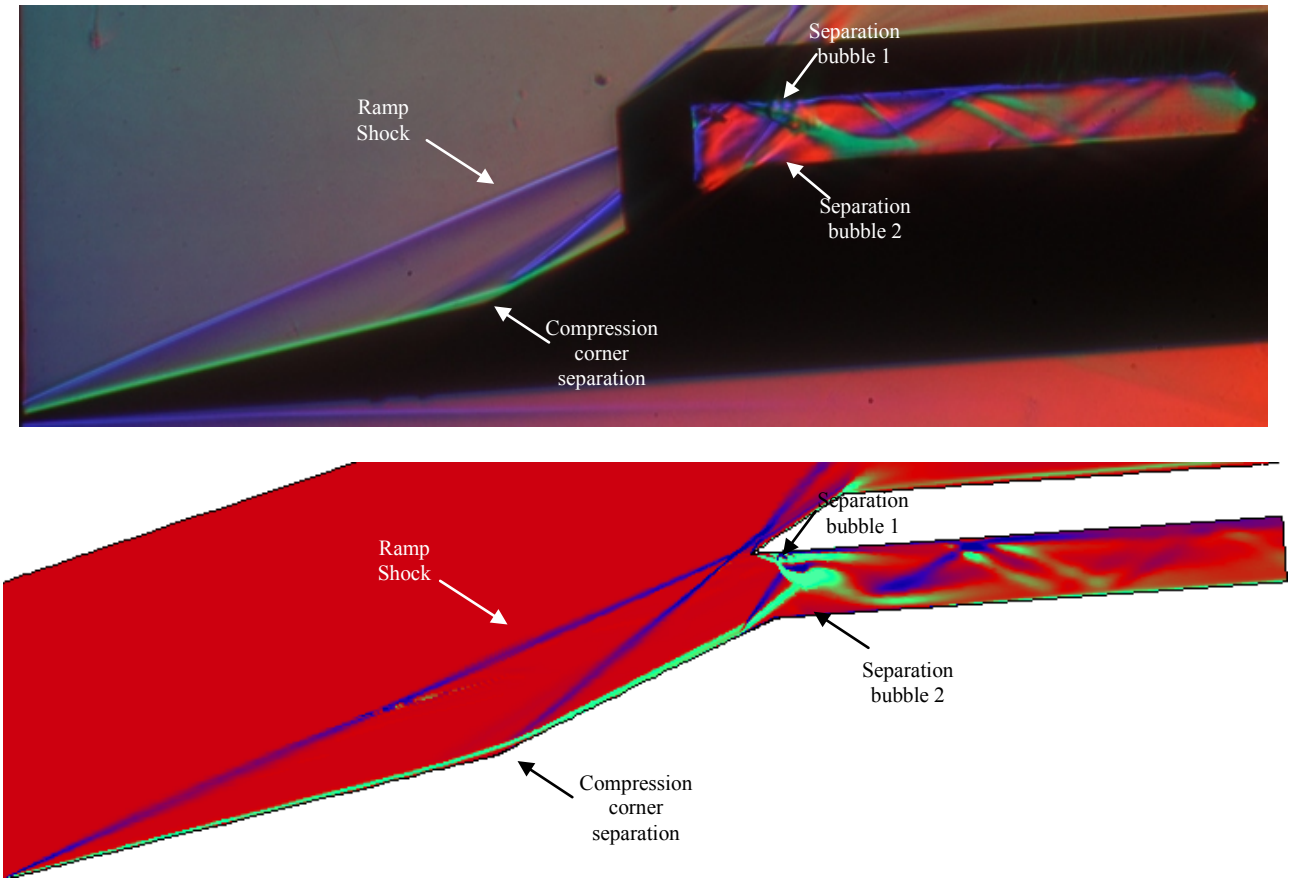

Fig. 6. [Top] Colour schlieren image of AoA = 4deg case. [Bottom] Numerical colour schlieren of AoA = 4deg case

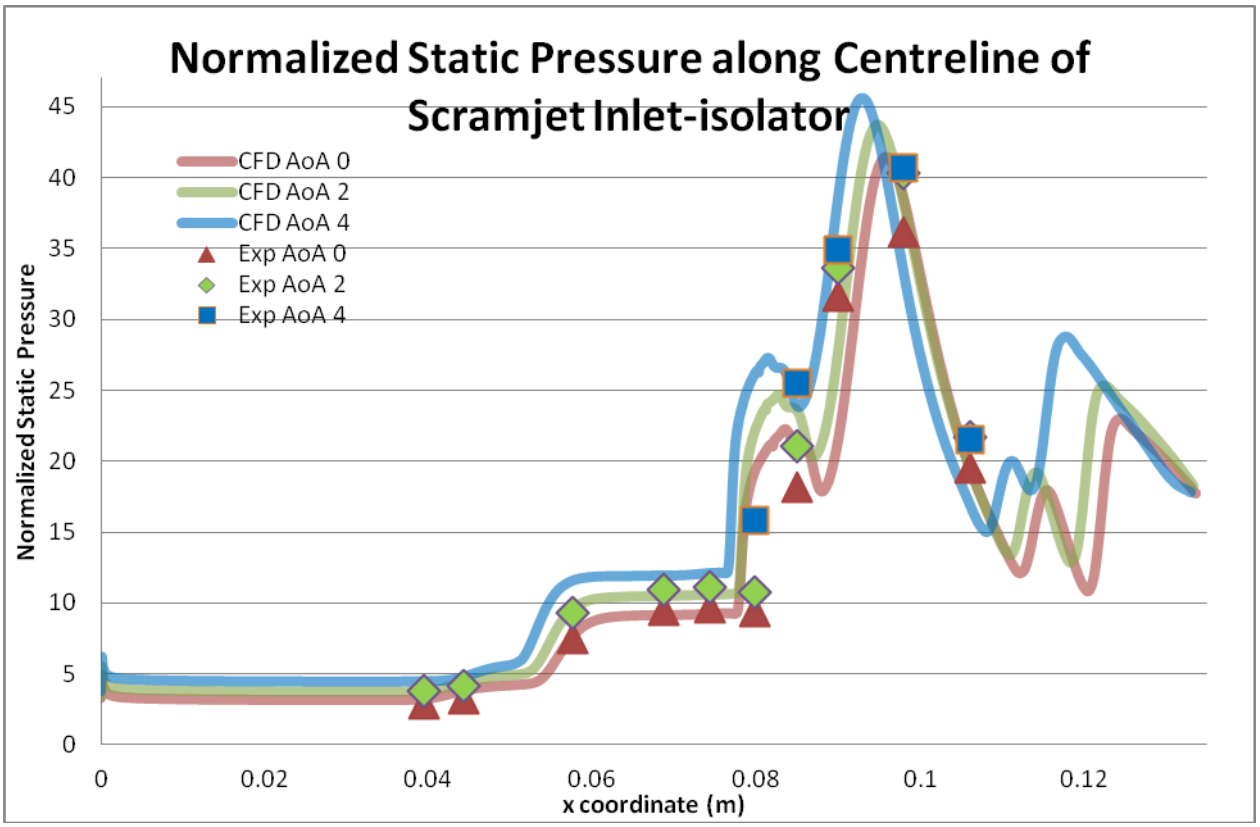

Fig. 7. Normalized static pressure along centreline of scramjet inlet-isolator for baseline, AoA = 2deg and AoA = 4 deg

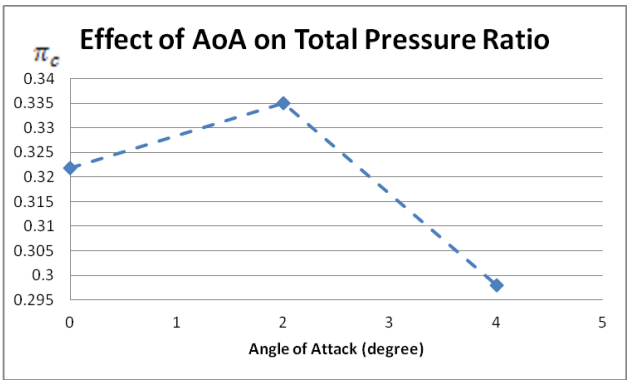

Fig. 8. Effect of AoA on Total Pressure Ratio

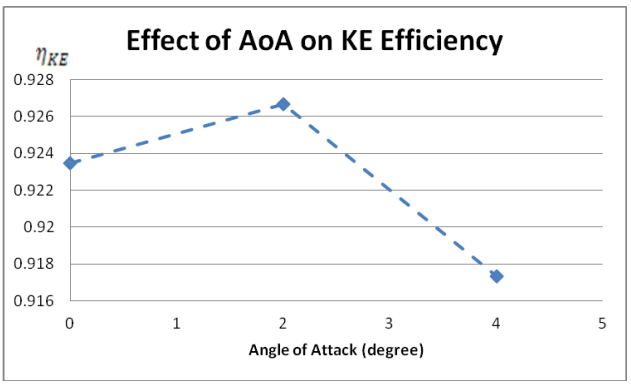

Fig. 9. Effect of AoA on Kinetic Energy Efficiency

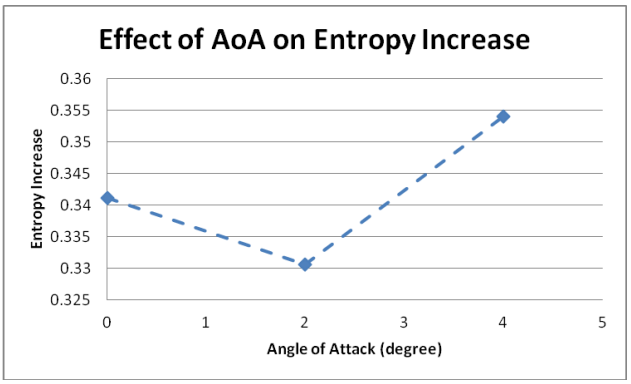

Fig. 10. Effect of AoA on Dimensionless Entropy Increase